Theor Chem Acc (1997) 96:176–194

Theoretical
Chemistry Accounts

Global potential energy surfaces for the lowest two $^1A'$ states of ozone

G. J. Atchity, K. Ruedenberg

Ames Laboratory, US Department of Energy and Department of Chemistry, Iowa State University, Ames, IA 50011, USA

Received: 10 January 1996 / Accepted: 2 January 1997

Abstract. The global features of the potential energy surfaces of the lowest two $^1A'$ states of ozone are established and detailed information is determined for the critical regions. Contour maps are generated on a variety of planes and curved surfaces cutting through the two energy surfaces in various directions to obtain a full understanding of the three-dimensional characteristics of both surfaces. Perimetric internal coordinates are used so that the three atoms are treated on an equal footing.

The $1^1A'$ state, the ground state, has a ring minimum and three equivalent open minima, all lying in C_{2v}-restricted coordinate spaces. Direct dissociation to $O_2 + O$ is only possible from the open minima. The lowest energy path from the ring minimum first leads to an open minimum before going to dissociation. The transition states between the ring minimum and the open minima also have C_{2v} symmetry. Close to these transition states lie the three open minima of the $2^1A'$ state, which has no ring minimum. Isomerization between the open minima is highly unlikely in the ground state, but not excluded in the excited state. Both states dissociate into the same state of $O_2 + O$, namely the ground state $O(^3P) + O_2(^3\Sigma_g^-)$ whose energy lies between that of the $1^1A'$ and $2^1A'$ open minima. There exists an extended, interestingly shaped region in coordinate space in which the two states come very close to each other. It contains an intersection seam between the two states consisting of four branches connected by three knots. Radiationless transitions between the two states can be expected.

Key words: Ozone – Potential energy surfaces – conical intersections

1 Introduction

Ozone has become particularly important because of its life-protecting ultra-violet absorption in the upper atmosphere. But it has also attracted attention because of its toxicity in big-city smog and its potential as a high-energy-density material. A comprehensive review of the experimental information on ozone until 1987 has been given by Steinfeld et al [1]. The lower potential energy surfaces (PES) of ozone dissociate into five combinations of the lowest states of the separated $[O_2 + O]$ system, viz. $[^3\Sigma_g^- + {}^3P]$, $[^1\Delta_g + {}^3P]$, $[^1\Sigma_g^+ + {}^3P]$, $[^3\Sigma_g^- + {}^1D]$, $[^1\Delta_g + {}^1D]$ which lie, respective, 1.13 ev, 2.11 ev, 2.76 ev, 3.10 ev, and 4.08 ev above the ground state equilibrium conformation of O_3. Ozone has C_s symmetry and, under neglect of spin-orbit coupling, its lowest states fall into six separate systems: $^1A'$, $^1A''$, $^3A'$, $^3A''$, $^5A'$, $^5A''$ where the A' and the A'' states are, respectively, symmetric and antisymmetric with respect to reflections in the molecular plane.

Theoretical studies of various surfaces have been made in recent years. Several excited states of some of the mentioned systems are usually investigated in conjunction with the $1^1A'$ ground state. Triplet surfaces have been studied in Refs. [2], [4], [7], [10], and [17]. The remainder of Refs. [2–17] deals with singlet surfaces. Typically the focus of the investigations is a limited region of the nuclear coordinate space, in particular restricted to C_{2v} symmetry or to dissociation channels. Examinations of *global* surfaces are still outstanding.

The ground state equilibrium structure of ozone is an isosceles triangle with an apex angle of 116.3°. Since each of the three oxygen atoms can be at the apex, there are three equivalent such minima. Near each of these geometries, the molecule has four excited singlet states within about 6 eV of the ground state energy. Under the restriction of C_{2v} symmetry (which is that of the ground state minima) the excited states belong to the irreducible representations $^1A_1$, $^1A_2$, $^1B_1$, $^1B_2$, while the ground state belongs to $^1A_1$. When the molecule distorts to C_s symmetry, the A_1 and B_2 irreps become A' whereas A_2 and B_1 become A''. Upon deformation of the molecule to an equilateral triangle (D_{3h} symmetry), *all singlet states become very high in energy except one* $^1A_1$ state (in C_{2v} labeling) which is part of the ground state potential energy surface (1^1A_1). It represents, in fact, a fourth minimum on this surface and there are three corresponding ring-opening transition states with apex angles of close to 90°. The electronic structure of the 1^1A_1 ring minimum is

Correspondence to: K. Ruedenberg

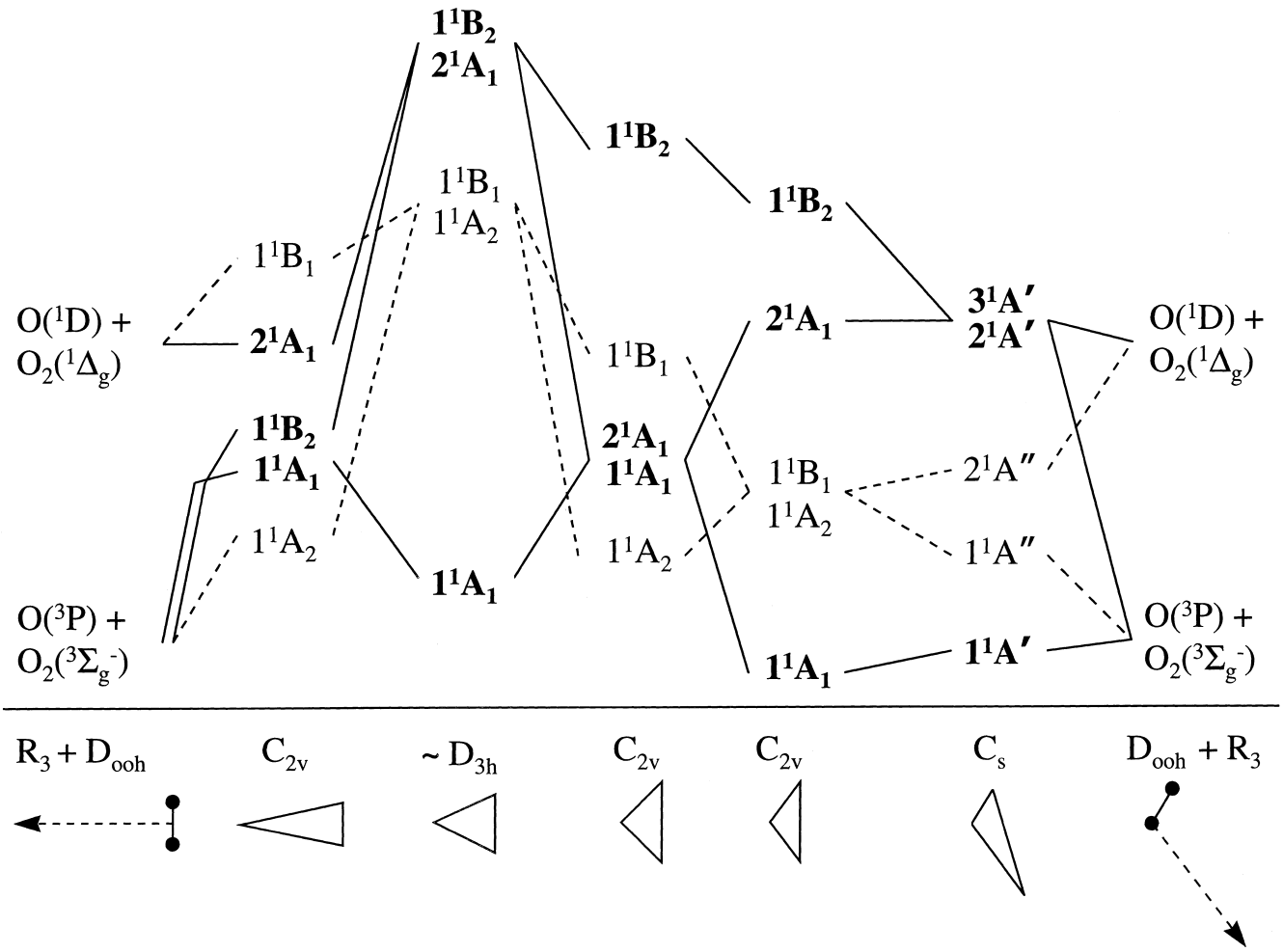

Fig. 1. Correlation diagram for the lowest singlet states of ozone. *Solid lines*: $^1A'$ system of PES. *Dashed lines*: $^1A''$ system of PES

related to the electronic structure of the *excited* 2^1A_1 state at the geometry of the 1^1A_1 *open* minimum.

Figure 1 displays a tentative correlation diagram for these four singlet states, including two dissociation paths into $O_2 + O$: One for the abstraction of the central atom, the other for the removal of an end atom. Due to crossings between the PES of various states (of different as well as like symmetry) for several geometries, the diagram is intrinsically complex. An attempt has been made to order the states qualitatively for various selected geometries. The figure is based on the results of the present investigation, on earlier unpublished calculations in this group, and on the results reported in Refs. [8] and [14].

We have shown and discussed elsewhere [9] that the lowest two $^1A'$ surfaces cross along a closed conical intersection seam in C_s symmetry and two points of this seam, both in C_{2v} symmetry, are indicated in Fig. 1: One is near the ring opening transition state of the 1^1A_1 surface, where the second $^1A'$ state is 2^1A_1; the other is on the way to the central-atom abstraction, where the second $^1A'$ state is $^1B_2$. Figure 1 also implies a conical intersection between $2^1A'$ and $3^1A'$ on the way to the end-atom abstraction, which is part of a seam that we anticipate on the basis of preliminary calculations. As yet, nothing is known about the $2^1A'$ state experimentally [1].

In view of these findings, an elucidation of the PES of these two states, $1^1A'$ and $2^1A'$, over larger regions of the internal coordinate space would be illuminating. The present investigation contributes such a study. Our principal aim is thus to obtain a credible picture of the global features of these two PES within a reasonable and sound approximation although, for the critical points, we shall also make contact with more elaborate calculations whose global application would be impractical. Developing procedures for bona-fide *ab-initio* elucidations of *global* potential energy surfaces seems to us an important objective in chemical physics since the determination of molecular properties at the critical points *only*, often does not suffice for an adequate understanding of reacting chemical systems.

2 Method

2.1 Wave functions

The reliability of theoretical predictions depends on the quality of the determined wave functions and, in the present context, it is necessary to strike a compromise between three competing desired objectives, viz., suffi-

cient accuracy for credible experimental predictions, sufficient flexibility for an unbiased description in different regions of the global internal coordinate space, and computational feasibility. Regarding the last objective, is has to be kept in mind that several hundred energy values may have to be determined on each two-dimensional cross section through a PES in order to identify the global features, and that the clarification of the critical regions may increase the effort by a substantial additional fraction. In the present case, about 2000 energies were determined on 15 coordinate planes for both surfaces.

2.1.1 Basis sets

Dunning's correlation-consistent VDZ (10s5p1d/3s2p1d) basis sets [18] were used for the three oxygen atoms. In Sect. 3, we shall see that multi-reference SDCI calculations yield reasonable values for the dissociation energies of $O_3 \rightarrow O_2 + O$ and $O_2 \rightarrow 2O$, which are notorious for being difficult to reproduce. We therefore believe this basis to be capable of generating credible results for the investigated potential energy surfaces. For higher excited states, complementation by diffuse orbitals is likely to be called for.

2.1.2 Configuration space

In order to guarantee the necessary flexibility over the various regions of the coordinate space we chose to determine the PES within the full valence space MCSCF approximation (FORS, Valence CASSCF [19]). For ozone, these wave functions contain 4067 CSFs in C_{2v} symmetry and 8027 CSFs in C_s symmetry. Moreover, since two states of the same symmetry are to be determined, the calculations were based on state-averaged energy minimizations (SA-FORS calculations), giving equal weights to both states and using the same orbitals for each. In Sect. 3, we shall compare the results obtained from these wave functions with those of more elaborate wave functions at selected points. It will be seen that the FORS wave functions yield the energy differences between the ring minimum, the open minimum, and the transition states with sufficient accuracy to be able to provide a credible elucidation of the PES.

The full valence space MCSCF wavefunction does not yield good quantitative values for the dissociation energies $O_3 \rightarrow O_2 + O$ and $O_2 \rightarrow 2O$, which, so far, have not been reproduced well with any medium-size configuration expansion. The corresponding points require, therefore, correction along the lines discussed in Sect. 3.

All calculations were performed with the MOLPRO program of Werner and Knowles [20].

2.2 Energy surface in coordinate space

2.2.1 Coordinate space

In order to draw meaningful conclusions from energy surfaces, one requires internal coordinates which can be straightforwardly related to the molecular shape and, at the same time, provide an intelligible visualization of the surfaces in the internal coordinate space.

In order to obtain a presentation which exhibits the equivalent roles of the three nuclei, we choose the so-called perimetric coordinates in their scale-shape adapted form. If r_{12}, r_{23}, r_{31} are the three internuclear distances, then the perimetric coordinates s_1, s_2, s_3 are defined by

$$s_i = s - r_{jk}, \quad i,j,k = \text{cyclic}, \quad s = (r_{12} + r_{23} + r_{31})/2. \tag{2.1}$$

Their scale-shape adapted versions are

$$x_1 = (s_2 - s_1)/\sqrt{2}, \quad x_2 = (2s_3 - s_1 - s_2)/\sqrt{6}, \quad x_3 = s/\sqrt{3}, \tag{2.2}$$

and it is readily seen that $\xi_1 = (x_1/s)$ and $\xi_2 = (x_2/s)$ depend only upon the angles of the molecular triangle. Thus, when the circumference of the molecule is fixed, then x_3 is constant and x_1 and x_2 describe the molecular shape. The area covered by the latter two parameters is the inside of an equilateral triangle including its borders. The explicit relationship between this parameter space and the molecular geometries are discussed in detail in the preceding paper [21].

Figure 2 exhibits the x_1–x_2 plane of these coordinates, perpendicular to the x_3 axis. In addition to the axes (x_1, x_2), additional axes (x_1', x_2') and (x_1'', x_2'') are also indicated which are obtained from (x_1, x_2) by rotations through $+120°$ and $-120°$, respectively.

Since all three nuclei are identical, the PES have C_{3v} symmetry with the x_3 axis being the threefold axis [21]. The entire PES can therefore be obtained from the section in the area that is shaded in Fig. 2 (between the negative x_2 and the positive x_2'' axes) by applying the symmetry operations of C_{3v}. Hence, energies have to be

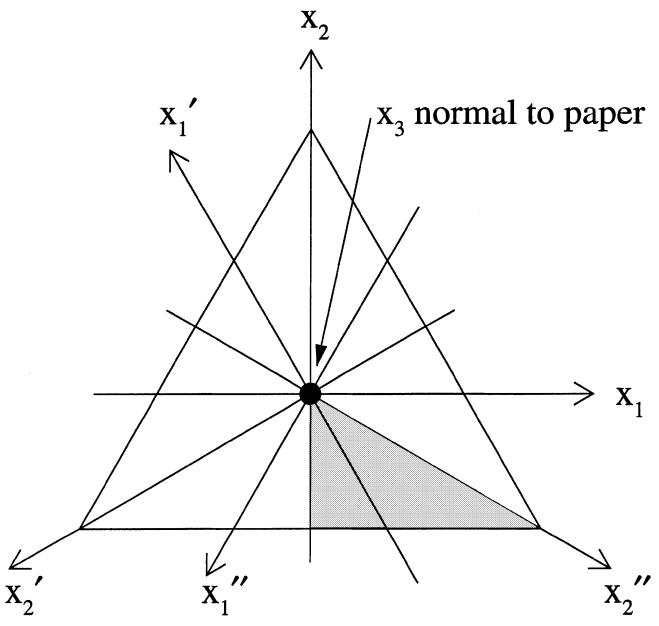

Fig. 2. Scale-shape adapted perimetric coordinates (x_1, x_2, x_3). *Shaded area*, region of independent energy values in ozone

calculated only in one-sixth of the global internal coordinate space.

In order to visualize the dependence on the three nuclear positions equivalently, we decided to determine cross sections through the PES on planes $x_3 = s/\sqrt{3} = r/(2\sqrt{3}) = \text{constant}$ (corresponding to molecules with fixed circumference) which cover the region of interest. Calculations were made on 15 such planes defined by the values of r going from 4 Å to 6.8 Å in steps of 0.2 Å. The relation of these values to relevant molecular confirmations is seen from Table 1.
The 15 coordinate planes correspond thus to the s values

$$s = 2.0, 2.1, \ldots, 3.4 \text{ Å}. \tag{2.3}$$

Four of these planes are illustrated on Fig. 3 with respect to the perimetric coordinates s_1, s_2, s_3.

On each of the 15 planes, energies were calculated on a grid of points located at distances of 0.1 Å in each direction – and confined to the unique shaded area indicated in Fig. 2. Only a few calculations were made, however, in the corners of the coordinate triangles where two atoms approach each other closer than about 80% of the O_2 bond length (≈ 0.96 Å) and the energy becomes correspondingly high. The larger the value $s = \text{const}$, the smaller is, of course, the fraction of the entire coordinate triangle taken up by these difficult-to-access corners. The number of points at which energies were calculated varied from 55 for $s = 2$ Å to 158 for $s = 3.4$ Å. Approximately 1500 energies were determined in total for this global scan. The closer examination of the various critical regions required energies at about an additional 500 points.

Table 1. Molecular circumference (Å) for some geometries of O_3

Confirmation	r_{12}	r_{13}	r_{23}	r
Ground state Open minimum	2.214	1.305	1.305	4.824
Ground state Ring minimum	1.476	1.476	1.476	4.428
Transition state between the above ($O_2 + O$) in C_{2v}	1.208[a]	2.796[b]	2.796[b]	6.800

[a] Equilibrium bondlength of O_2
[b] Distance used later on to represent the near-dissociated system

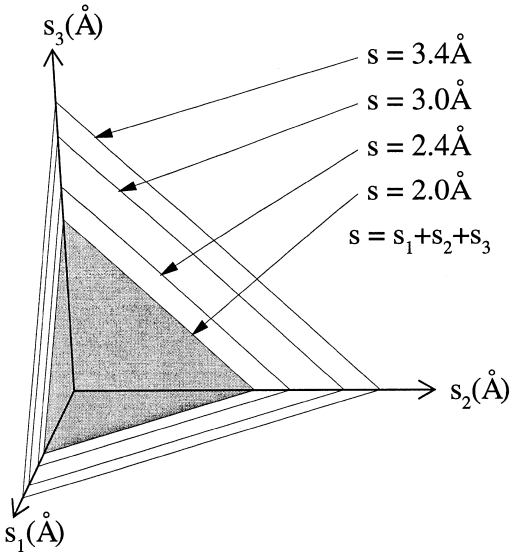

Fig. 3. Four planes $s = \text{constant}$ in the perimetric coordinate system. *Shaded plane*, $s = 2.0$ Å

2.2.2 Interpolation

Interpolation of the calculated energy values is a necessity for the graphical depiction and analysis of PES. There are at least two essential reasons for this. One is the preparation of energy contours in a coordinate plane. Contouring algorithms are routinely predicated upon the function values to be plotted being offered on a rectangular grid which is equidistant along each coordinate axis. Moreover, in order to obtain good, smooth contours, the grid has to be quite a bit denser than the pristine grid mentioned above on which energies were actually evaluated. The contouring grid has therefore to be derived from the pristine grid by interpolation. Another need for interpolation arises when one wishes to determine energy values and contours on planes or surfaces other than $x_3 = \text{constant}$. Such a change in the viewing directions is an important tool for fully visualizing the three-dimensional behavior of a PES. To cut across a PES at various inclinations and with various origin displacements appears to be the only way to gain a complete understanding of its global character, since only limited insight can be obtained by generating three-dimensional energy contour surfaces perspectively. For these reasons, energies were calculated on 15 planes $x_3 = \text{constant}$, so that a grid with elementary displacements of 0.1 Å was available for interpolation in all three coordinate directions.

Bi-variate interpolation techniques are still evolving and an ideal "method for all seasons" has not yet been found [22]. Different methods are useful under different conditions. If the pristine data are given on a rectangular grid that is equidistant in each coordinate direction, then cubic B-spline procedures are applicable and usually do a fine job [23]. This is useful for limited areas of the coordinate space. However, since we obtain data points in the full coordinate space by means of the C_{3v} operations, applied to one-sixth of the data, we do not have such a grid for the global coordinate space. Moreover, it is often desirable to augment the original data set by additional denser grids in critical regions of the PES. For a pristine data set of this kind, one must use "scattered data interpolation" methods [24] which are still topics of research. We have used several methods: a triangulation method by Akima [25] and two methods based on the weighted superposition of local interpolation functions, one based upon the method of Shepard [26], another by Franke [27]. The performance of the various procedures depended upon the distribution and the homogeneity of the data.

The bivariate interpolation methods rarely reproduced exact pristine data and, not infrequently, had problems in generating smoothly curved contours when

plotted. It must however be acknowledged that quantum chemical potential energy surfaces have a tendency to change their geometric characteristics very rapidly in the regions of greatest interest and are therefore not easy objects for interpolation. The development of bivariate and, subsequently, multi-variate interpolation algorithms optimally suited for molecular potential energy surfaces would seem to be a subject deserving further investigative attention.

3 Critical features of the potential energy surfaces

Before proceeding to the global examination of the PES of the $1^1A'$ and $2^1A'$ states, it seems expedient to discuss the critical features of the two surfaces found by our calculations.

The ground state $1^1A'$ has four minima: three open minima, each of C_{2v} symmetry and belonging to the $^1A_1$ irrep, with the apex angle of 116° located at one of the three oxygen nuclei, and one ring minimum with D_{3h} symmetry. To each of the open minima, there leads a transition state from the ring minimum, with an apex angle of about 84°. Very close to each of these transition states, the excited 2^1A_1 state has a minimum and, in the immediate vicinity, is part of a $1^1A'$–$2^1A'$ intersection seam in C_s symmetry. The ground state dissociation can occur along six pathways, two from each of the open minima, with one of the end atoms moving away under approximate preservation of the apex angle. The dissociation from an excited state minimum occurs in a somewhat similar fashion. Both the $1^1A'$ and the $2^1A'$ states have the same dissociation limit $[O(^3P)+O_2(^3\Sigma_g^-)]$ (see Fig. 1), whose energy lies between those of the $1^1A'$ and $2^1A'$ minima. There exists, therefore, a barrier along the dissociation path on the $2^1A'$ surface. The calculations also reveal a barrier to dissociation on the $1^1A'$ ground state surface. This feature is in agreement with recent analysis of experimental data [28], as will be elaborated below.

The discussed energetic relationships are quantitatively represented in Fig. 4. Figure 4a exhibits the results from the state-averaged full valence state MCSCF (SA-FORS) calculations. Figure 4b exhibits the results of the corresponding internally contracted multi-reference singles and doubles CI (ICMRSDCI) calculations where the full FORS space was complemented by all internally contracted single and double excitations within the (3s2p1d) basis mentioned in Sect. 2.1 [29]. This configuration space is of dimension 446,977 (the dimension of the uncontracted SDCI space is about 21×10^6). The full quantitative data of the various calculations are listed in Table 2. Table 3 lists the parameters of the various optimized geometries.

It is seen from Table 2 and Fig. 4 that the energy differences between the ground state minima and the transition state between them are reproduced similarly by both the FORS wave functions, the SA-FORS wave functions, and the ICMRSDCI wave functions.

The vibrational frequencies at all ground state minima have been determined in our previous investigation [9] (which covered a smaller region of the PES) and they turned out to be in good agreement with the frequencies from highly correlated calculations near the minima [30]. Since the present work is performed within the same full active configuration space as that in Ref. [9] (albeit with a better contracted AO basis set), very similar values will be obtained.

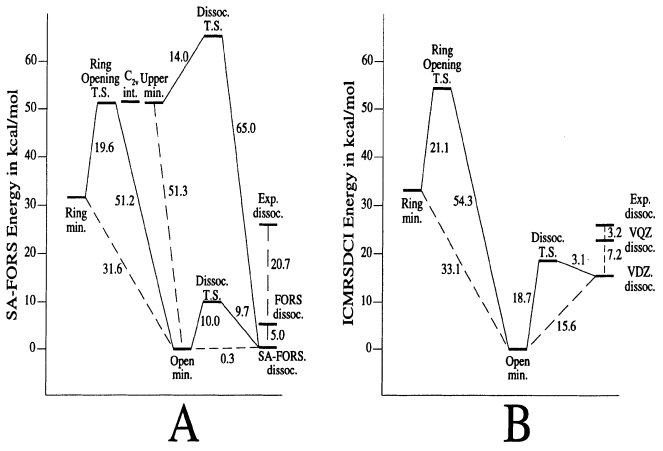

Fig. 4. Critical energy differences for the $1^1A'$ and the $2^1A'$ states of ozone. *A* FORS calculations; *B* ICMRSDCI calculations. Energies are in kcal/mol. See text

Table 2. Comparison of ground state energy differences obtained from various configurational approximations[a]

	Ring minus open	R-O TS[b] minus ring	(O_2+O) minus open	Dissoc TS[c] minus (O_2+O)	2O minus O_2
FORS[d]	51.03	33.82	8.46	13.46	141.66
SA-FORS[e]	50.41	31.25	0.45	15.54	141.66
ICMRSDCI[f]	52.84	33.73	24.83	4.98	165.06
Experiment			41.43		191.65
FORS - SA FORS	0.39	2.73	8.01	−2.08	0
ICMRSDCI -FORS	1.81	−0.08	16.37	16.37	23.40

[a] All energies in millihartree. 1 millihartree ≈ 0.6kcal/mol.
[b] Ring-opening transition state
[c] Calculated transition state to dissociation
[d] Single-state calculations
[e] State-averaged calculations
[f] ICMRSDCI wave function using FORS reference and FORS optimized orbitals

Table 3. Geometry parameters of critical points of the ground state of ozone

	O—O Bond Length	O—O—O angle
Open min.	1.298Å	116.32°
Ring-opening TS	1.431Å	83.86°
Ring min.	1.470Å	60.0°
Dissociation TS[a]	1.211Å, 1.720Å	113.59°
O_2	1.2075Å	–

[a] All critical points except the dissociation transition state possess C_{2v} symmetry

The results for the dissociation energy, on the other hand, confirm the well-known fact that the calculation of the $O_3 \rightarrow O_2 + O$ dissociation presents a considerable challenge (as does the $O_2 \rightarrow 2O$ dissociation). The dissociation energy of the single-state FORS wave function yields only 20% of the experimental value, and the state-averaged FORS wave function gives only 1%. Even the ICMRSDCI value with the same VOZ basis is seen to recover only 60% of the experimental energy difference. It was only by means of an ICMRSDCI calculation with Dunning's much larger correlation consistent [5s4p3 d2f1g] VQZ basis set, yielding almost 3 million contracted configurations, that we generated a dissociation energy of 36.31 mh; nearly 88% of the experiment. This result agrees well with what is probably the best reliable value to date, namely 36.8 mh, which was obtained by Stanton et al. with CCSDT-1 wave functions and a [5s3p2d1f] basis set [31].

Whereas the FORS wave function yields a sizable barrier to dissociation on the $1^1A'$ surface, as mentioned earlier, a much smaller barrier is obtained with the corresponding ICMRSDCI calculation at this FORS-determined geometry, and the optimization of the transition state geometry on the ICMRSDCI surfaces would lower the barrier even further, if indeed it is preserved. However, even with the VDZ-based MRCI calculations, the energy is found to rise *very* sharply upon removal of the end atom and it is therefore likely that a slight barrier will manifest itself in all calculations. A slight barrier had also been found by other theoretical workers [5,8]. In fact, such a small barrier has recently been deduced from fitting a sophisticated empirical PES to the actual spectroscopic data [28]. We therefore draw two inferences from the present results: (1) the reaction channel for dissociation essentially corresponds to one end atom moving away with the apex angle remaining between 113° and 116°, and (2) along this reaction coordinate, the PES rises very sharply to a small transition state of less than 5 mh, reaching the energy of $(O_2 + O)$ when one of the bonds in O_3 has been stretched by only 33% over the equilibrium distance.

4 Global features of the $1^1A'$ potential energy surface

As mentioned in Sect. 2.2, energies of the two states were calculated on the 15 planes $s = x_3/\sqrt{3} = r/2 = 2.0, 2.1, \ldots, 3.4$ in the perimetric coordinate space, four of which were shown in Fig. 3.

4.1 Minima and transition states

Contours of the lower state $1^1A'$ on 12 of the above-mentioned planes are exhibited in Fig. 5. All features of this PES can be deduced from the following markings. Since the global (open) minima have an energy of $E_0 = -224.501$ h, *all contours on all panels correspond to energy values* $E_0 + k \times 20$ mh ($k = integer$, $20\,\text{mh} \approx 0.54\,\text{eV} \approx 12\,\text{kcal/mol}$). *They can be related to each other by reference to the bold contours which correspond to the energy* $E_0 + 60$ mh *on all panels*. The shaded areas denote regions within which the energy goes downhill to local minima *on that panel* ("basins") and all contours which are boundaries of basins have the same energy value *on any one panel*. The energy values go up for the contours in the unshaded regions. No contours are drawn for energy values larger than $E_0 + 200$ mh since they become too dense. This occurs when two atoms get substantially closer to each other than the O_2 equilibrium distance 1.21 Å. These regions are indicated as dotted areas on all panels.

It is seen that, for s values ≤ 2.5 Å, each PES cross section has one ring minimum in the center, three equivalent open minima, and three saddle points leading from the ring minimum to the open minima. *The minimum* (*as a function of s*) *of each of the three open minima* occurs for $s = 2.412$ Å with an energy of $E = E_0$; these minima represent the equivalent global equilibrium structures and are indicated on the panel for $s = 2.4$. *The minimum of the ring minima* (*as a function of s*) occurs for $s = 2.214$ Å with an energy of $E = E_0 + 51$ mh; it is the metastable ring equilibrium structure and is indicated on the panel for $s = 2.2$. The *minima of the saddle points* occur for $s = 2.396$ Å with an energy of $E = E_0 + 82$ mh; they are the transition states from the ring structure to the open structures and are indicated on the panel for $s = 2.4$. For a value of s between 2.5 Å and 2.6 Å, the ring minimum disappears and, for all larger s values, the PES has a dome in the center region.

4.2 Dissociation

Between $s = 2.6$ Å and 2.7 Å, one can see the onset of dissociation: each of the open minima splits into two, moving away from the original C_{2v} position, under approximate preservation of the apex angle (See Fig. 6 of Ref. [21]). For large s values, the dissociated system $[(O^{(1)} - O^{(2)}) + O^{(3)}]$ has $r_{12} = R(O_2) = 1.21$ Å, so that

$$x_2 = (-s_1 - s_2 + 2s_3)/\sqrt{6} = (2s - 3r_{12})/\sqrt{6} = s\sqrt{2/3} - 1.21\sqrt{3/2}. \tag{4.1}$$

Hence, x_2 is constant on a panel $s = \text{constant}$. For $s = 3.4$ Å, it has the value $x_2 = 1.29$ Å which is not too different from the minima on the panel for $s = 3.4$ Å. Counting of contours on panels $s = 2.6$ Å to 3.0 Å reveals the existence of a barrier with respect to dissociation on this surface, at about $s = 2.7$ Å with a barrier height of about 16 mh. This is in agreement with Fig. 4a and with Table 2. Most likely, the relatively large size of this barrier is connected with the failure of the MCSCF wave function in predicting the dissociation energy $O_3 \rightarrow O_2 + O$ correctly, as was discussed in Sect. 3. On Fig. 4b and Table 2, we saw indeed that the barrier is greatly reduced at the MRSDCI level of calculation. However, as mentioned in Sect. 3, a small barrier towards dissociation probably exists.

A better view of the channel for this dissociation is obtained by looking at the contours on a surface in coordinate space, which approximately contains the dissociative reaction path. Such a surface is defined in Fig. 6. Figure 6a shows the s_1, s_2 coordinates of several critical points of the $1^1A'$ surface in the s_1–s_2 coordinate

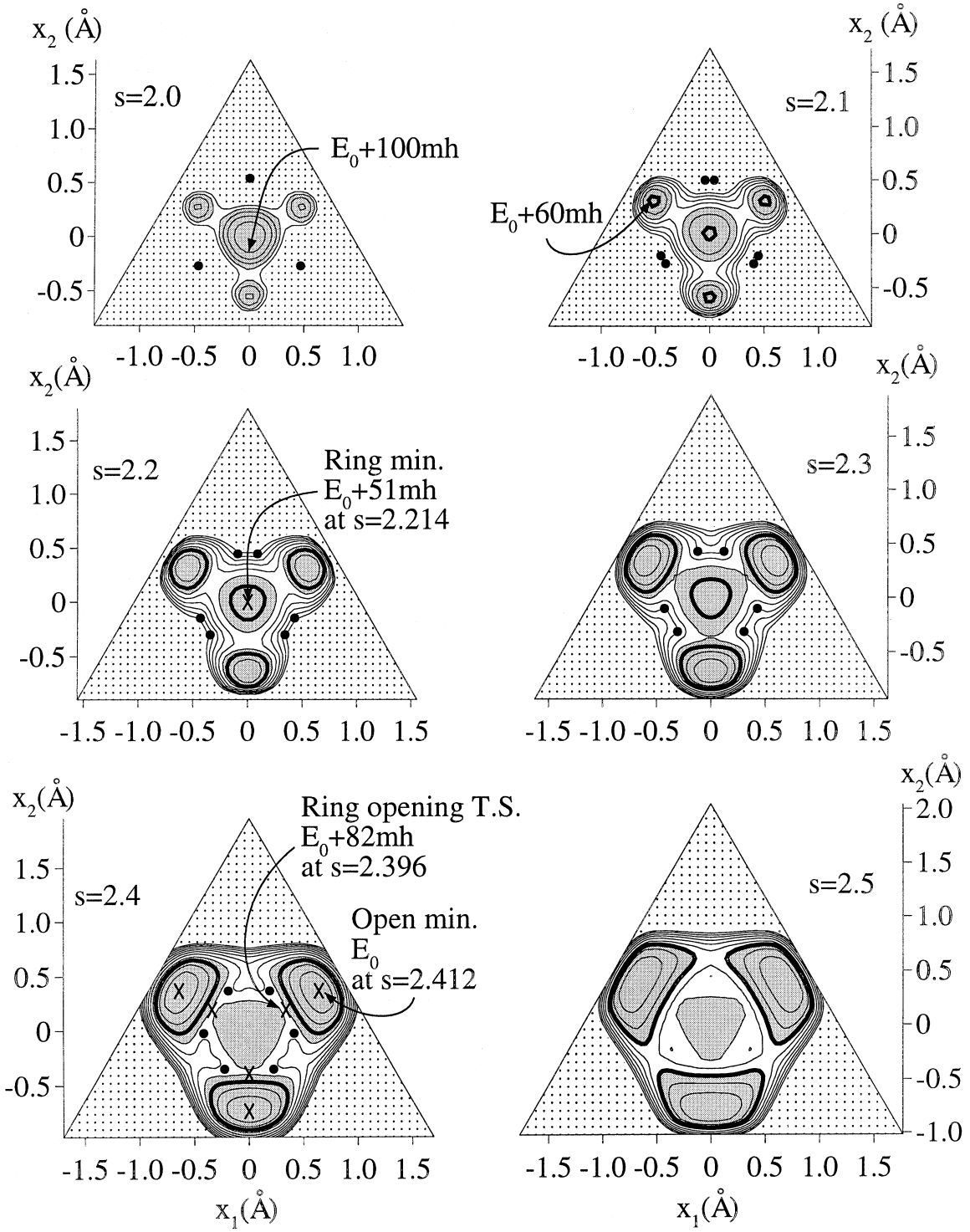

Fig. 5. a 1^1A_1 state PES contours in planes normal to the x_3 axis: $s = 2.0$ Å to $s = 2.5$ Å *Markings:* see text Sect. 4.1

plane. Namely, the (s_1, s_2)-values for two open minima and the corresponding transition states, as well as the dashed line $s_1 + s_2 = R(O_2) = 1.21$ Å, for the dissociated system $O_2 + O$ (with nucleus $O^{(3)}$ being removed). Figure 6a furthermore shows a parabola drawn in a least-mean-square fashion through these critical point projections. As a surface on which to plot PES contours, we now choose the parabolic cylinder section which is parallel to the s_3 axis, perpendicular to the s_1–s_2 plane, and intersecting the s_1-s_2 plane in the parabola just described. Such a cylinder is shown in Fig. 6b, which also illustrates the intersection of this cylinder section with two planes $s =$ constant.

The contours of the $1^1A'$ PES on this cylinder section are shown on the upper panel of Fig. 7. As on Fig. 5, the bold lines indicate the contours $E_0 + 60$ mh and the

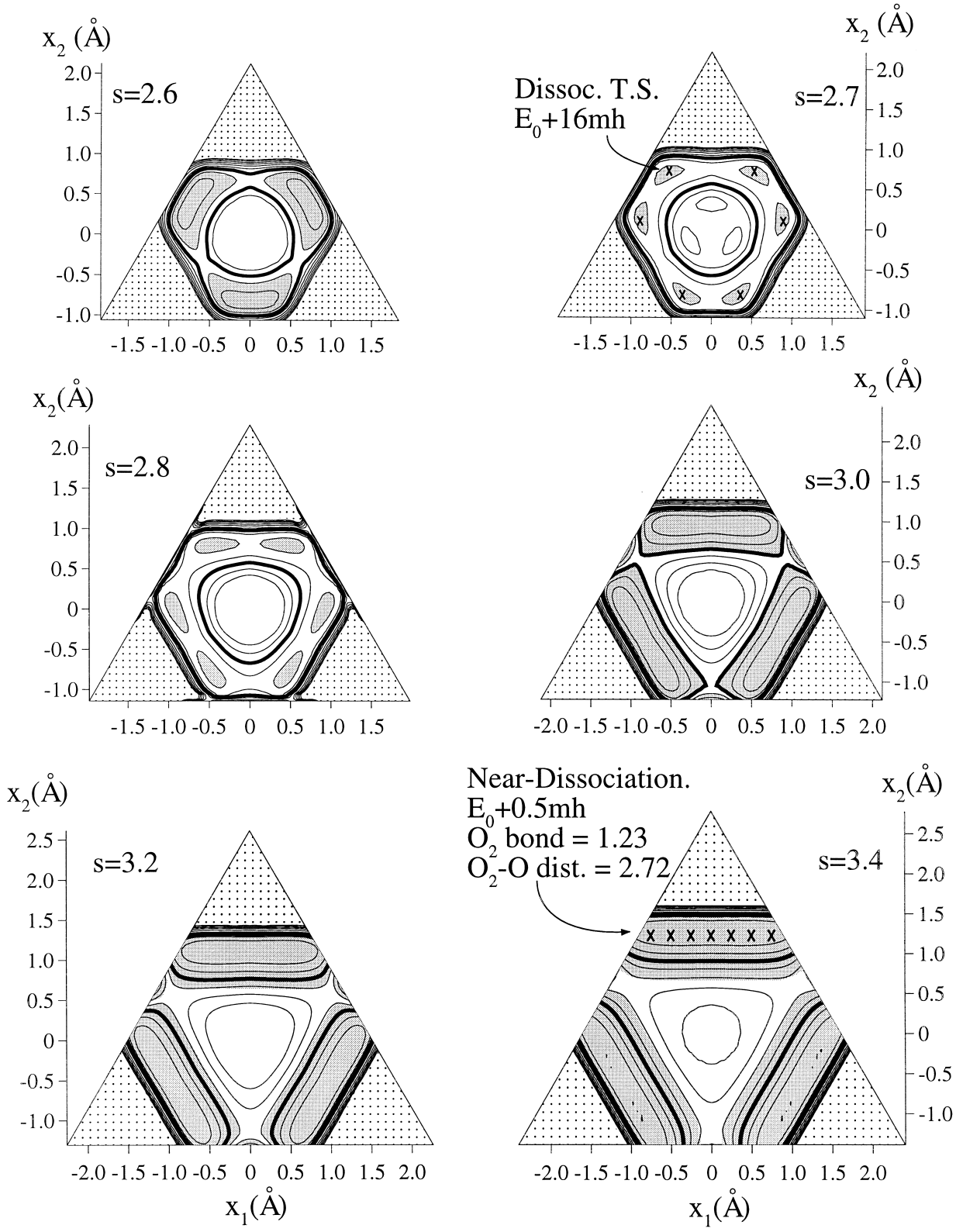

Fig. 5. b 1^1A_1 state PES contours in planes normal to the x_3 axis: $s = 2.6$ Å to $s = 3.4$ Å. *Markings* as in **a**

shaded areas indicate basins. The increment between contours is, however, only 5 mh and the dotted area covers the region $E > E_0 + 100$ mh. The intersections of the parabolic cylinder with four planes s = constant are indicated by dashed straight horizontal lines and the same intersection lines are shown on the smaller, lower panels, representing contours on corresponding planes s = constant taken from Fig. 5.

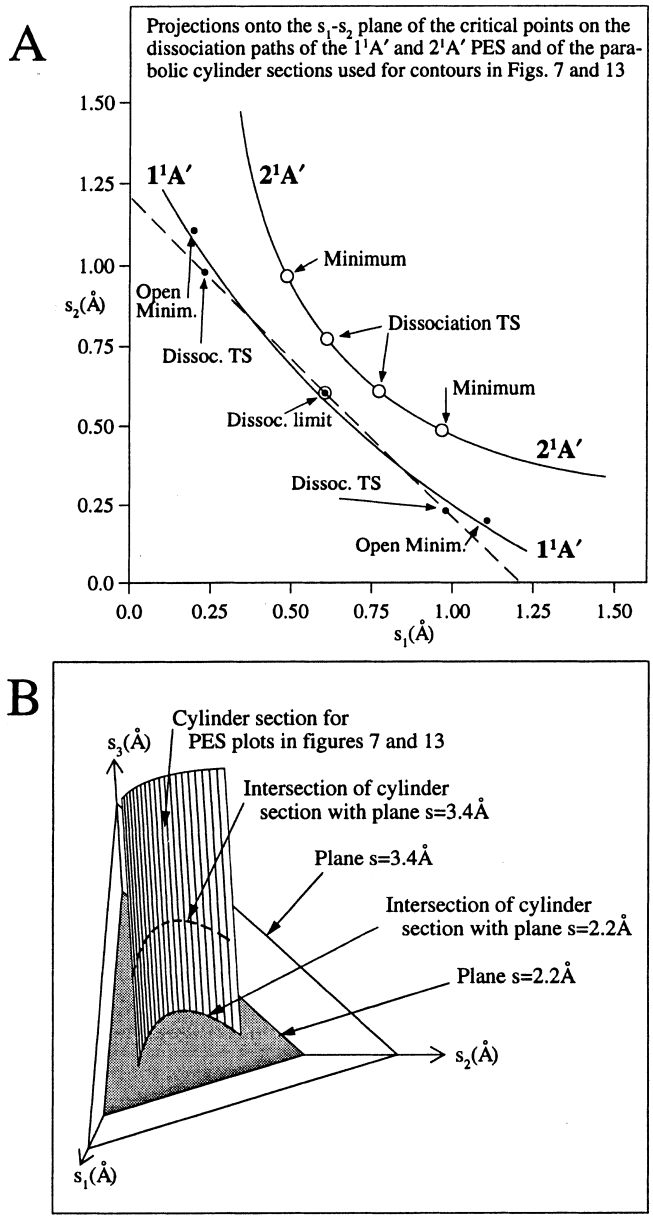

Fig. 6. Cylinder sections in perimetric coordinate space for dissociative contour plots considered in Figs. 7 and 12

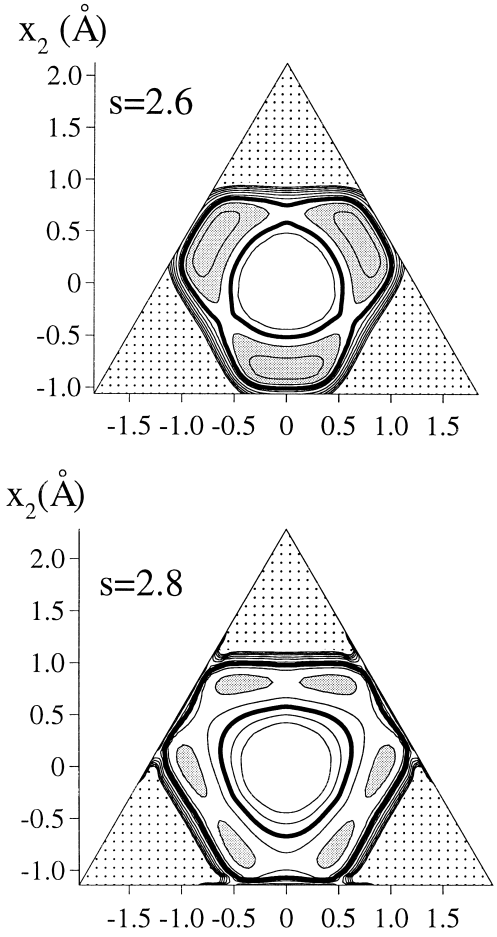

Fig. 7. *Upper panel*: contours of $1^1A'$ PES on the cylinder defined in Fig. 6 for this state. Lines of *heavy dots* are on C_{2v}-conserving planes; *Lower panels*: contours on the planes $s = 2.4, 2.6, 2.8, 3.4$. The *dashed lines* on all panels show the curves on which the cylinder of the upper panel intersects with the planes of the lower panels

The dissociation channels from the two open minima are quite apparent. An important inference from this PES contour plot is that *there is no realistic option of avoiding dissociation in favor of isomerization from one open minimum to another*.

4.2.1 Is dissociation from the ring minimum into $O_2 + O$ possible without passing through an open minimum?

The contours of Fig. 5 are somewhat awkward for recognizing whether or not a direct dissociative reaction path exists from the ring minimum without first going to an open minimum, e.g. by abstraction of the central oxygen. In order to answer this question, we determined PES contours on three planes *containing the* x_3 *axis*, i.e. *perpendicular to the planes* $s =$ constant These planes, called A, B, C, are shown perspectively in Fig. 8, where the axes $(x_1, x_2, x_1', x_2', x_1'', x_2'')$ are those which have been shown in Fig. 2. The PES contours on these planes are exhibited in Fig. 9, where the markings have the same meanings as those in Fig. 5. Since the panels A and C correspond to two, albeit different, C_{2v} subspaces, they show equivalent contours. On each of these two panels, one sees one of the open minima, the ring minimum and the saddle point on panel C between them. (This part of the plot is equivalent to Fig. 4 of Ref. [9a]). Comparing the region around this saddle point on panel C of Fig. 9 with that on panel $s = 2.4$ Å of Fig. 5, one sees that the C_{2v}-conserving normal mode pointing to the two minima is the *only* downhill mode in all three dimensions and that there exist *two* uphill normal modes, one C_{2v} conserving (in Fig. 9) and another C_{2v} symmetry breaking (in Fig. 5, panel $s = 2.4$ Å). This saddle point is therefore indeed a transition state.

In Fig. 9 panels A and C there occurs, however, another saddle point, marked by a hollow dot, whose steepest descent line leads to a dissociation corresponding to abstraction of the central atom in a C_{2v}-conserving

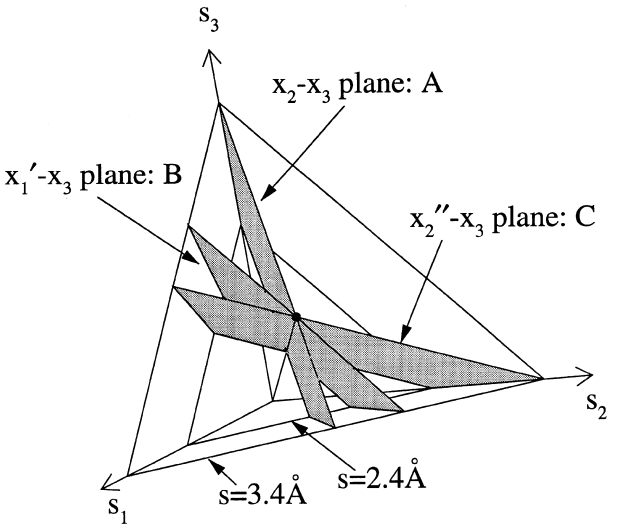

Fig. 8. Planes $ax_1 + bx_2 = 0$ in perimetric coordinate space used for contour plots in Fig. 9 and in Fig. 13

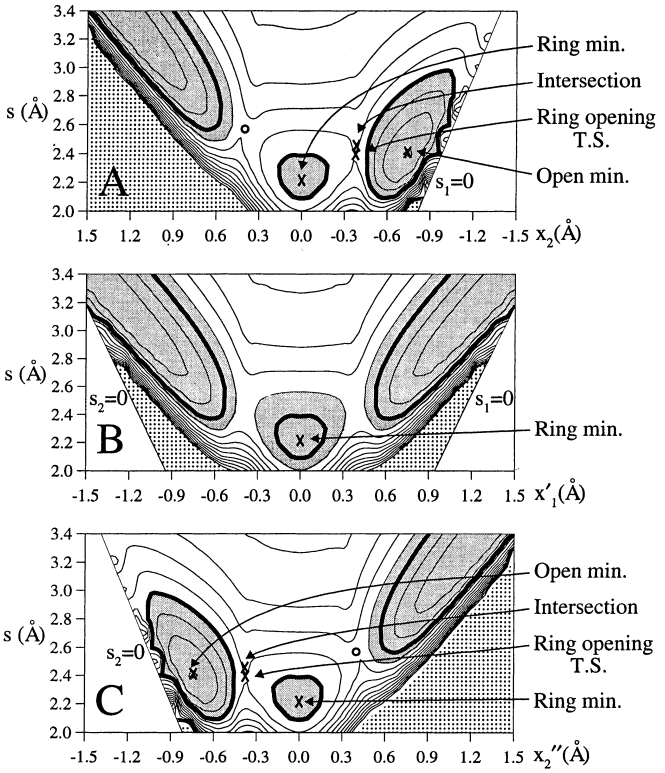

Fig. 9. $1^1A'$ state PES contours in planes containing the x_3 axis, defined in Fig. 8. See text

subspace. In addition to this C_{2v}-conserving downhill mode at this saddle point, which occurs at about $s = 2.6$ Å in panel C, one finds, however, a *second*, C_{2v} symmetry breaking, downhill mode, namely on the panel for $s = 2.6$ Å of Fig. 5, heading towards two open minima. This saddle point is therefore not a transition state. Moreover, it is almost 20 mh higher than the transition states towards the open minima. One must therefore conclude that most reaction trajectories which might start out towards a C_{2v}-conserving abstraction of a central oxygen will turn around and end up in one of the open minima. Hence, dissociation from the ring structure is expected to go through one of the open minima.

The contours on panel B of Fig. 9 are intermediate between panels A and C. They give an indication how these contours deform into each other if one slowly rotates the plotting plane around the x_3 axis from A to C. The saddle points on panel B of Fig. 9 are not saddle points on Fig. 5.

4.3 Linear structures

Linear arrangements of the three atoms correspond to the sides of the coordinate triangles of Fig. 5. It is seen that, for $s \leq 2.6$ Å, the *isosceles* linear structure, corresponding to the midpoints of the triangle sides, are the ones with the lowest energies and represent saddle points with respect to inversion of the molecule under constant circumference. For panels with $s \geq 3$ Å, where we approach dissociation, the lowest energy occurs for two atoms at the O_2 equilibrium distance and the third atom, collinearly, a long distance away.

In Fig. 9, the linear molecules are represented by the lines marked as $s_1 = 0$ (corresponding to $O^{(1)}$ lying between $O^{(2)}$ and $O^{(3)}$) and $s_2 = 0$ (corresponding to $O^{(2)}$ lying between $O^{(1)}$ and $O^{(3)}$). Panels A and C of Fig. 9 represent C_{2v}-preserving planes and, therefore, the lines $s_1 = 0, s_2 = 0$ correspond to the *isosceles* linear molecules which, as noted above, are saddle points on the panels for $s \leq 2.6$ Å on Fig. 5. It is seen from Fig. 9 panels A, C that the saddle points with the lowest energy occur at about $s = 2.5$ Å. These points are therefore transition states with respect to inversion, with a barrier of about 60–70 mh and bond lengths of about 1.25 Å.

On the other hand, it is apparent from Fig. 8 that the lines $s_1 = 0$ and $s_2 = 0$ in of Fig. 9 correspond to linear molecules where the distances between the central atom and the two end atoms are in a ratio of 2 : 1 (See Sect. 4.2 of Ref. [21]). When the shorter of these distances is equal to the O_2 bond length of 1.21 Å, then the larger one will be 2.42 Å and s = half, the circumference, will be 3.63 Å. It is apparent that the (extrapolated) minima on the lines $s_1 = 0$ and $s_2 = 0$ of Fig. 9b occur just about for this value of s. The similarity of these minima for large s values with those in panels A and C reflects the independence of the dissociated system from the location of the dissociated oxygen atom. The near-dissociation minimum on the lines $s_1 = 0$ of panel B is reached from the global open minimum of panel A by a path penetrating panels intermediate between A and B, in agreement with the earlier discussion of this dissociation.

5 Global features of the $2^1A'$ potential energy surface

The contours of the $2^1A'$ state on planes s = constant are displayed in Fig. 10. The *method* of marking is the same as that for the $1^1A'$ state in Fig. 5. In fact, the

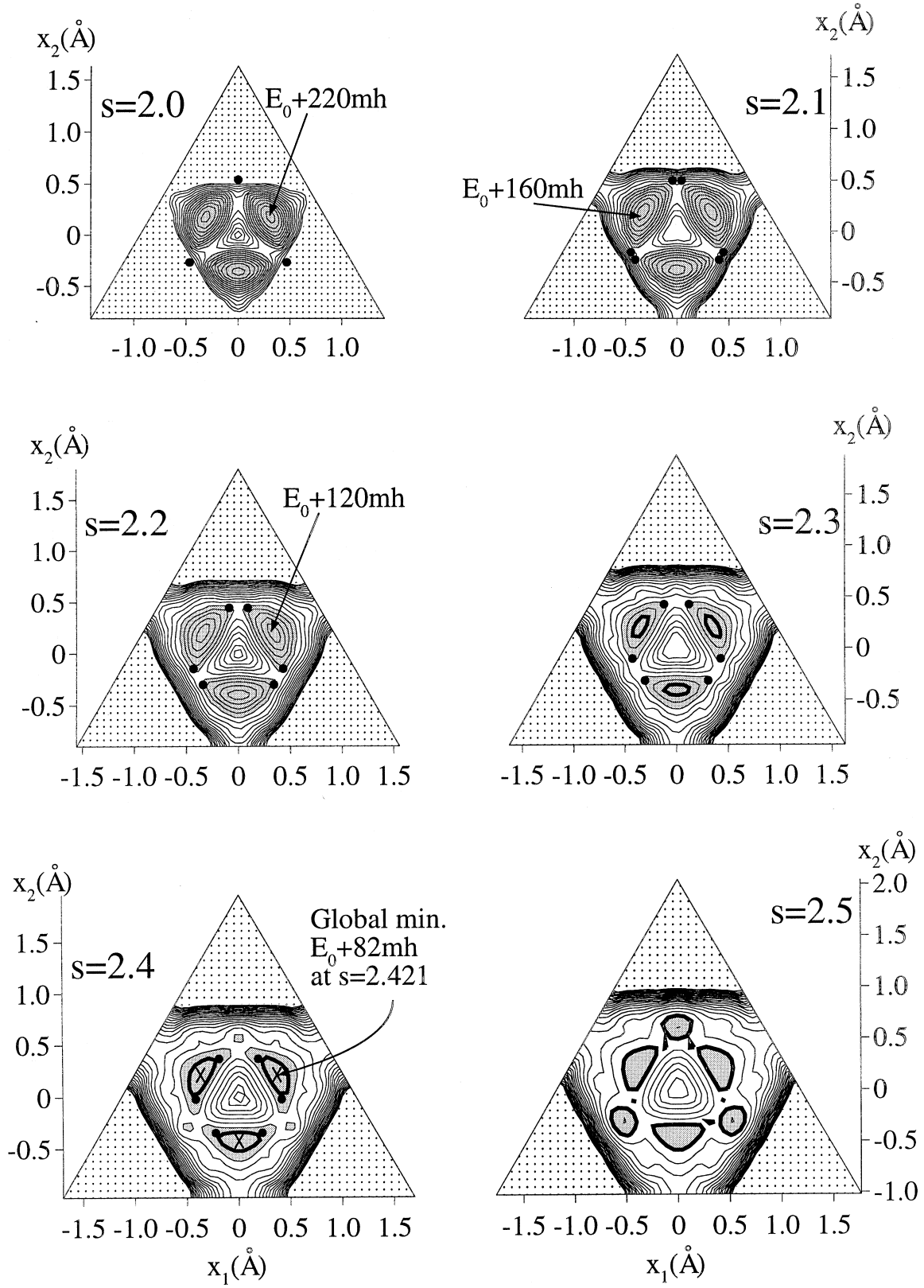

Fig. 10. a $2^1A'$ state PES contours in planes normal to the x_3 axis: $s = 2.0$ Å to $s = 2.5$ Å. *Markings*: see text in introduction to Sect. 5

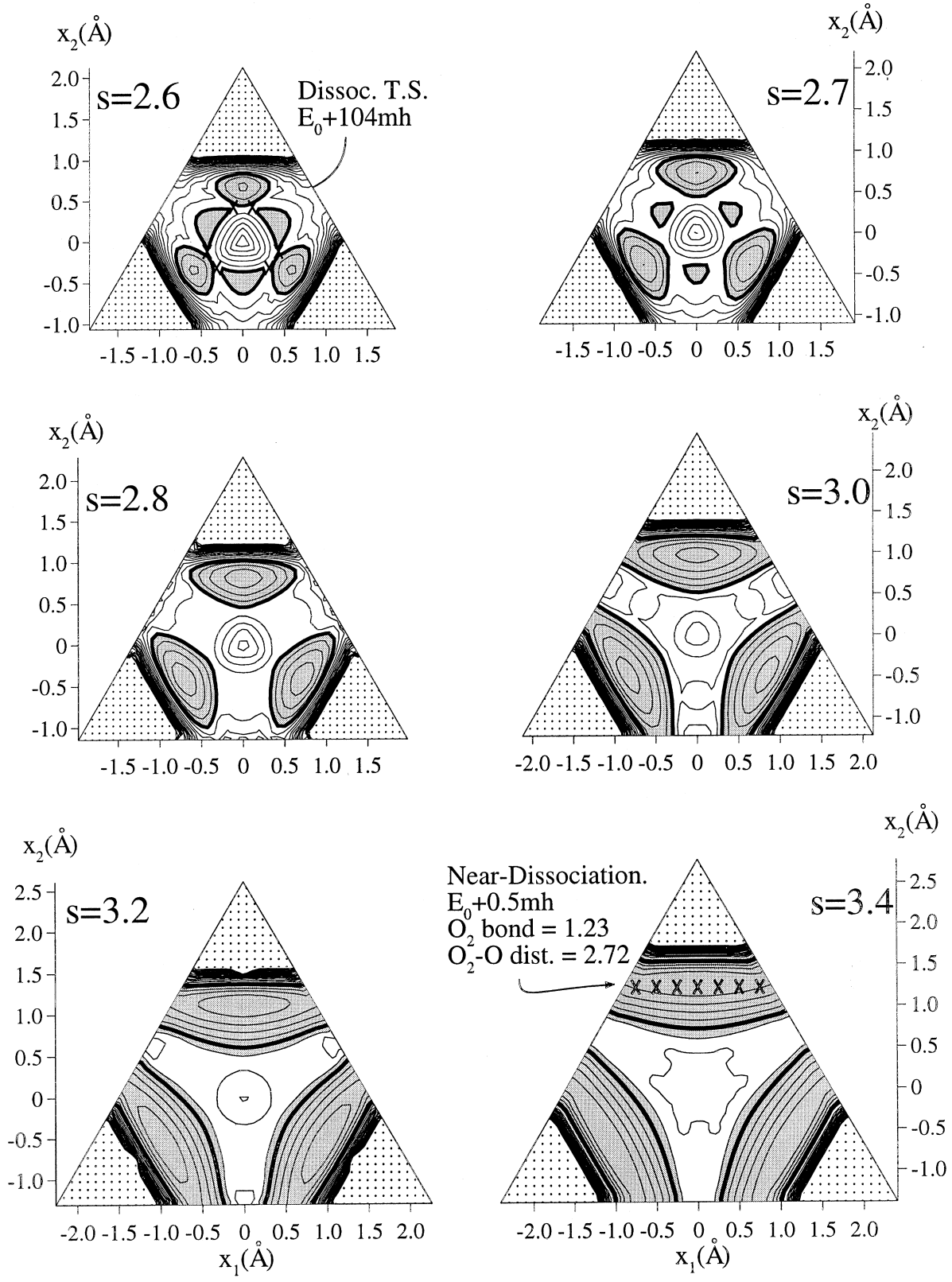

Fig. 10. b $2^1A'$ state PES contours in planes normal to the x_3 axis: $s = 2.6$ Å to $s = 3.4$ Å. *Markings* as in **a**

energy increment between contours (20 mh) is the same in both figures and some contours in Fig. 10 have the same energy as some contours in Fig. 5. However, the bold contours in Fig. 10 correspond to the energy $E_0 + 100$ mh, i.e. they are 40 mh higher than the bold contours in Fig. 5. Similarly, the dotted corner regions start at a higher energy ($E_0 + 500$ mh compared to $E_0 + 200$ mh in Fig. 5). Here , E_0 still denotes the global minimum of the ground state.

5.1 Minima

On all panels $s = 2.0$ Å to 2.7 Å, the PES cross sections exhibit three minima corresponding to open structures (i.e. with apex angles $> 60°$). The minimum (as a function of s) of these minima occurs for $s = 2.421$ Å with an energy of $E_0 + 82$ mh. These global minima of the $2^1A'$ state are indicated on the panel for $s = 2.4$ Å. As mentioned earlier, their locations are very close to the transition states connecting the ring minimum and the open minima on the ground state PES.

In contrast to the ground state, the $2^1A'$ PES has no ring minimum. In fact, its energy is quite high for conformations near the equilateral triangle structure.

5.2 Dissociation

On the panel $s = 2.4$ Å one notices the appearance of a second set of three minima, corresponding to *acute* molecular triangles with C_{2v} symmetry. These minima become more pronounced on the panels $s = 2.5$ Å and 2.6 Å The transition, on a panel $s = \text{const}$, from one of the previous minima (open triangle structures) to one of the presently considered minima (acute triangle structures) corresponds to a change in electronic structure. Indeed, for the acute triangle minima, the electronic wave function belongs to the irreducible representation $^1B_2$. With increasing values of s, corresponding to one oxygen moving further and further away from the O_2 fragment left behind, these minima steadily decrease in energy and reach their lowest value for $s = \infty$, where they end up with the same ($O_2 + O$) configuration as the ground state (see Fig. 1). (For $s = 3.4$ Å, this state is, however, less close to being a dissociated system than $1^1A'$ was, in as much as the minimum energies in Fig. 10 are not yet constant along lines parallel to the triangle sides.) The minima for the open triangle structure, on the other hand, become less and less deep with increasing s and finally disappear. Consequently, there exists a dissociation path from the global minimum of the $2^1A'$ PES for $s = 2.421$ Å to the near dissociated system for $s = 3.4$ Å. The transition state for this path occurs at $s = 2.6$ Å where the saddle point between the two types of minima (for $s = \text{const}$) reaches its minimum, with a barrier of $(104\,\text{mh} - 82\,\text{mh}) = 22\,\text{mh}$.

Two successive enlargements of the panel for $s = 2.6$ in the region around this transition state are shown in Fig. 11, where the energy contour increments are 1 mh and 0.5 mh, respectively, and the shadings indicate basins with energy values $E \leq E_0 + 103$ mh. It can be seen that the two transition states lie within 0.2 Å of each other. If both would move by 0.1 Å towards each other, then they would coalesce into one, on the x_2 axis with C_{2v} symmetry at the position marked by an asterisk in Fig. 11, and it would become a transition state for isomerization between two equivalent minimum structures rather than for dissociation. It would seem that, even with the critical region as it is in Fig. 11, there is some probability for the molecule to undergo isomerization from one open minimum to another when starting out on this reaction path.

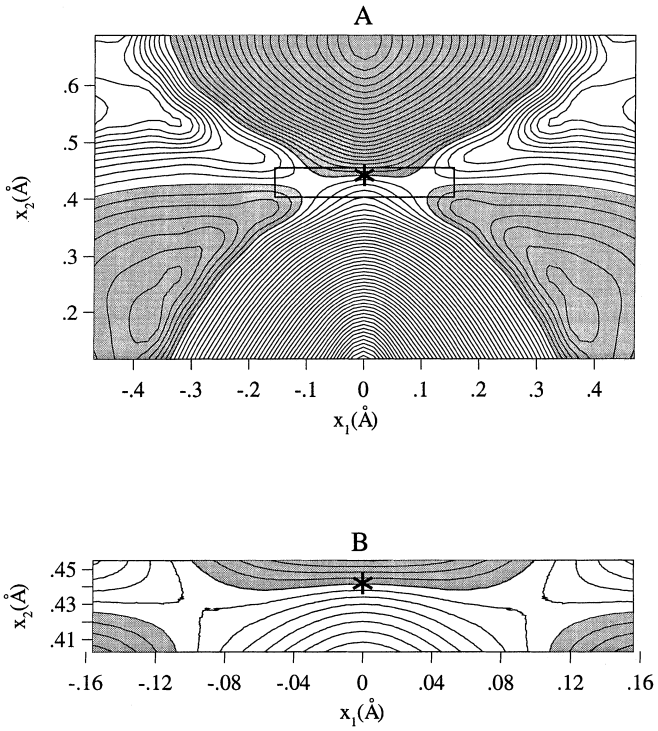

Fig. 11. *A* Enlargement of the $2^1A'$ state PES for $s = 2.6$ near the dissociative transition state. Increment = 1 mh. *B* Further enlargement of the area in the rectangle indicated in *A*. Increment = 0.5 mh

As in the case of the $1^1A'$ PES, this dissociation channel can be better recognized by contours on a parabolic cylinder perpendicular to the s_1–s_2 plane. In Fig. 6A, the s_1, s_2 coordinates of the critical points of the $2^1A'$ state and the LMSQ parabola through them are also indicated. As before, we consider contours on a parabolic cylinder, such as shown in Fig. 6B, but now intersecting the s_1–s_2 plane in the parabola associated with the 2^1A_1 state. It should be noted that, on it, the dissociated system has an O_2 bond length of 1.37 Å, i.e. somewhat larger than the O_2 equilibrium bond length of 1.21 Å. The contours on this cylinder section are displayed in Fig. 12 where the markings are very similar to those in the analogous Fig. 7 for the $1^1A'$ surface. The contours confirm that the two transition states are close to having the characteristics of *one* transition state in C_{2v} connecting the two open minima, while a third downhill branch splits off at a right angle toward the

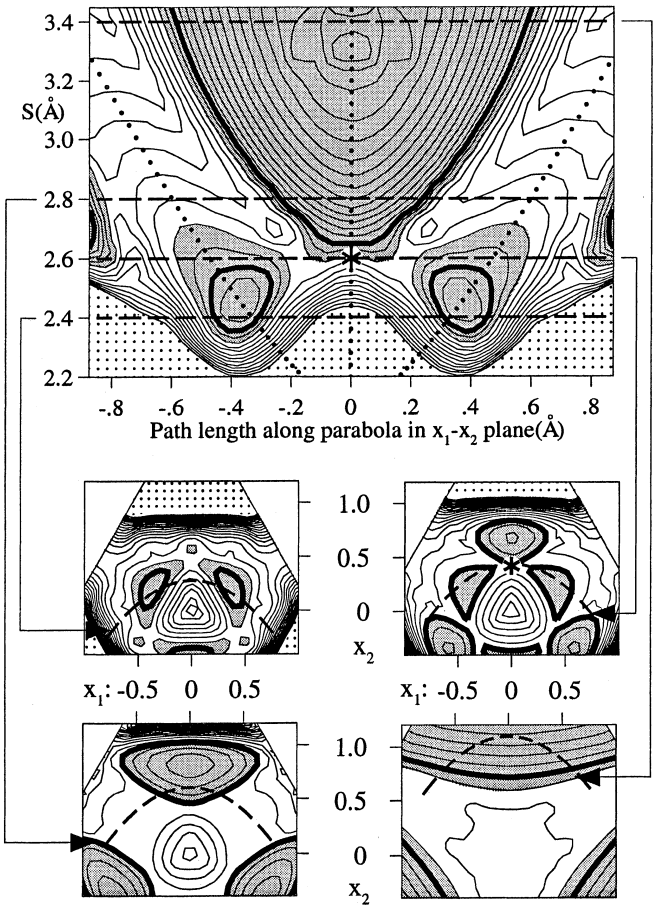

Fig. 12. *Upper panel*: contours of $2^1A'$ PES on cylinder defined in Fig. 6 for this state. Lines of *heavy dots* are on C_{2v}-conserving planes. *Lower panels*: contours on the planes $s = 2.4, 2.6, 2.8, 3.4$. The *dashed lines* on all panels show the curves on which the cylinder of the upper panel intersects with the planes of the lower panels

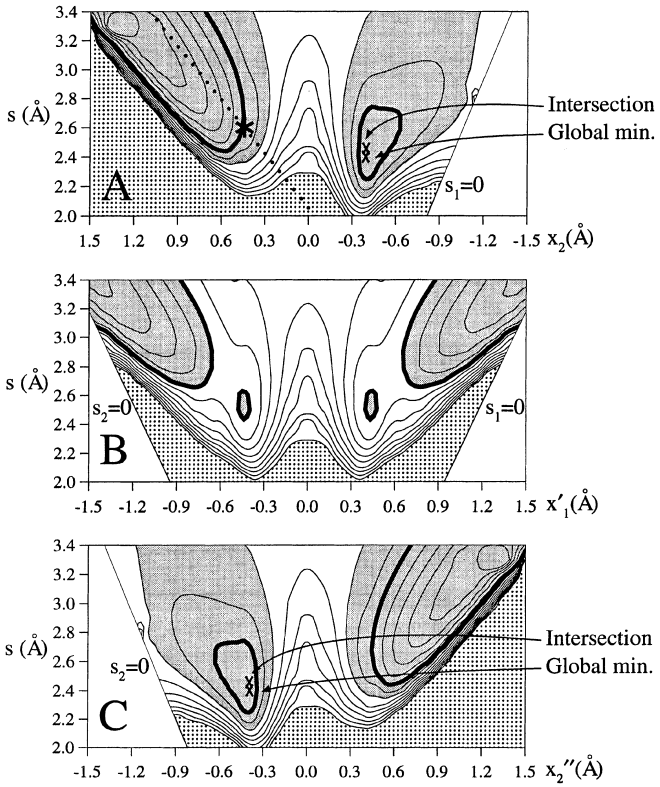

Fig. 13. $2^1A'$ state PES contours in planes containing the x_3 axis defined in Fig. 8

dissociated system. This latter, C_{2v}-conserving, downhill steepest descent path originates on a ridge from the center of the coordinate plane (corresponding to the high-energy ring geometries) and changes into a valley very close to the aforementioned transition states. At this valley-ridge inflection point [32] the second derivative of the energy vanishes in the C_{2v} symmetry-breaking x_1 direction.

As was the case for the $1^1A'$ state, further insight into the dissociation can be obtained from the contours on the three planes A, B, C specified in Fig. 8. Cross sections of the $2^1A'$ PES in these planes are displayed in Fig. 13. The contours in this figure are analogous to those shown in Fig. 9 for the $1^1A'$ state and have similar markings. The dotted line in panel A indicates the intersection of the C_{2v}-conserving plane A of Fig. 8 with the cylinder of Fig. 6B discussed in the previous paragraph. Since, on that cylinder, C_{2v} symmetry implies $s_1 = s_2 = r_{12}/2 = 1.37/2$, the dotted line in Fig. 13A is given by the equation

$$x_2 = (-s_1 - s_2 + 2s_3)/\sqrt{6} = (2s - 3r_{12})/\sqrt{6} = 0.816s - 1.678. \quad (5.1)$$

In Fig. 12, which displays the contours on the cylinder of Fig. 6, this same intersection is the vertical dotted line in the center. Moreover, in both Fig. 12 and Fig. 13 the point

$$x_1 = 0, \quad x_2 = 0.442\,\text{Å}, = \sqrt{3}x_3 = 2.6\,\text{Å} \quad (5.2)$$

is indicated by an asterisk. This is the point we found earlier as the point midway between the two transition states in Fig. 11 where it is also marked by an asterisk. It now becomes apparent that, in Fig. 13A, the steepest descent reaction path from this point to dissociation does not deviate too much from the cylinder constructed in Fig. 6.

5.3 Linear structures

An examination of the triangle sides in Fig. 10 and of the lines $s_1 = 0$ and $s_2 = 0$ in Fig. 13 leads to conclusions regarding the linear structures of the $2^1A'$ state, which are similar to those found for the $1^1A'$ state. Namely, there exist linear isosceles transition states with respect to inversions from one minimum to another at about $s = 2.8$ Å, corresponding to two equal bond lengths of 1.4 Å, with a barrier of about 65 mh. For large values of ($s \geq 3$ Å), the minimum of the linear molecules corresponds to an oxygen molecule in its ground state and an oxygen atom at a large distance.

6 Energy difference between the two states

6.1 Global features

We know from previous investigations [9b] that the $1^1A'$ state and the $2^1A'$ state intersect along a seam which forms a closed curve, looping around the x_3 axis in our coordinate system. We have also shown [9a] that, at least in C_{2v}, intersection is of the sloped type [33] and that the two surfaces seem to stay close to each other over a somewhat extended range near the C_{2v} intersection point. Since, in such regions, there exists a high probability for radiationless transitions, it is of interest to know the actual *global extent* of the part of coordinate space where the energy between the two states is small.

Contours of the energy difference $\Delta E = [E(2^1A') - E(1^1A')]$ on panels $s =$ constant are therefore exhibited in Fig. 14. Note that, here, the markings are very different from those in the analogous Figs. 5 and 10 for the separate surfaces. Now, *the light areas denote the regions of low ΔE values, namely* $\Delta E < 20$ mh. In this area, there can be one more contour, namely $\Delta E = 5$ mh. Shaded is the area where $\Delta E > 20$ mh. The increment between contours is 15 mh. The bold contour corresponds to $\Delta E = 95$ mh. The dotted corner regions correspond to molecular geometries where two oxygen atoms approach each other closer than 0.8 Å $\approx 66\%$ of the O_2 bond length, where the energies of both states become extremely high.

An examination of all panels reveals that the shape of the light regions where the two states come close remains remarkably similar for practically all values of s.

6.2 Region of close approach

From Fig. 14, it is apparent that, in the three-dimensional coordinate space, the region of close approach represents a volume which is *schematically* drawn in Fig. 15. It is *approximately* the volume between two cylinders with radii 0.4 Å and 0.5 Å, the x_3 axis being the cylinder axis, and, joined to it, three sheet-like volumes within about 0.1–0.2 Å of those sections of the three C_{2v}-conserving planes which, starting at the aforementioned cylinder, go outward to the corners of the coordinate triangle of Fig. 2.

In order to gain a more accurate picture of the mutual approach of the two PES, we consider them as functions of a radial coordinate d and an angular coordinate ω, where

$$\mathrm{d} = (x_1^2 + x_2^2)^{1/2}, \quad x_1 = \mathrm{d}\sin\omega, \quad -x_2 = \mathrm{d}\cos\omega \qquad (6.1)$$

(see Fig. 16). According to Eqs. (3), (15) and (17) of Ref. [21], the radial coordinate can be expressed as

$$\mathrm{d} = (r_{12}^2 + r_{23}^2 + r_{13}^2) - (r_{12} + r_{23} + r_{13})^2/3. \qquad (6.2)$$

Figure 17 exhibits the energies of the two PES as functions of d for various values of ω (see Fig. 16) and for various values of the scaling coordinate s (= half the circumference of the molecule). For each panel $s =$ constant, we then determined by interpolation the points of closest approach and, by fitting these points with a function of the form

$$\mathrm{d}(\omega) = c_1 + c_2\sin 3\omega + c_3\sin 6\omega + c_4\sin 9\omega, \qquad (6.3)$$

we obtained the curve of closest approach $\mathrm{d} = \mathrm{d}(\omega)$ for each value of s. These curves are displayed in Fig. 18.

It can now be seen that Fig. 15 is really oversimplified. Whereas, for $s = 3.4$ Å, the shape of the region of close approach is indeed almost circular, it deforms with decreasing values of s and, for $s = 2.0$ Å, its shape is closer to that of a triangle with rounded corners. It is also noteworthy that the curves of Fig. 18 do not come close to the dotted corner areas indicated on Fig. 14.

6.3 Intersection seam

It stands to reason that the intersecting seam between the two states, which was a partial stimulus for the present investigation, is expected to lie in the volume of close approach depicted in Fig. 15.

In the companion paper [9b], we explicitly determine the intersection seam which loops around the x_3 axis, i.e. which runs in the cylinder-like section of Fig. 15. The panels of Fig. 17 contain four points, each one given by a set of values for (ω, s, d, E), that belong to this seam. They are indicated by heavy dots and they are manifestly located where the interpolated curves of the two surfaces come very close to each other. In Fig. 18, the heavy dots indicate the projection of the intersection seam on the x_1–x_2 plane, as given by Fig. 4 of the companion paper [9b]. This projection is seen to follow closely the Least-mean-squares approximations for $s = 2.3$. Intersection points are also indicated by heavy dots in Figs. 5, 10 and 14.

Moreover, it is found in Ref. [9b] that the intersection consists of four connected branches S_0, S_1, S_2, S_3. While the branch S_0 is the one just discussed, there is an additional branch in each of the three C_{2v}-conserving planes. These branches (S_1, S_2, S_3) lie in the sheet-like volumes of Fig. 15 which are fanning out from the cylinder to the triangle corners (see Fig 10 Ref. [9b]). The peculiar form of Fig. 15 is thus in complete agreement with the shape of the intersection seam determined in Ref. [9b]. Finally, it is also found in Ref. [9b] that, on the branches S_1, S_2, S_3, the two states belongs to different irreps of C_{2v}, namely $^1A_1$ and $^1B_2$, and this is presumably the case for the entire sheet-like parts of Fig. 15.

7 Summary

The global features of the potential energy surfaces and detailed information regarding their critical points have been established for the lowest two $^1A'$ states of ozone.

The ground state has a D_{3h} ring minimum and three equivalent open C_{2v} minima. A lowest-energy path leads from the ring minimum over a transition state to each open minimum. From each of these minima, two lowest-energy paths lead, under approximate preservation of the apex angle, to dissociation into $O_2 + O$, corre-

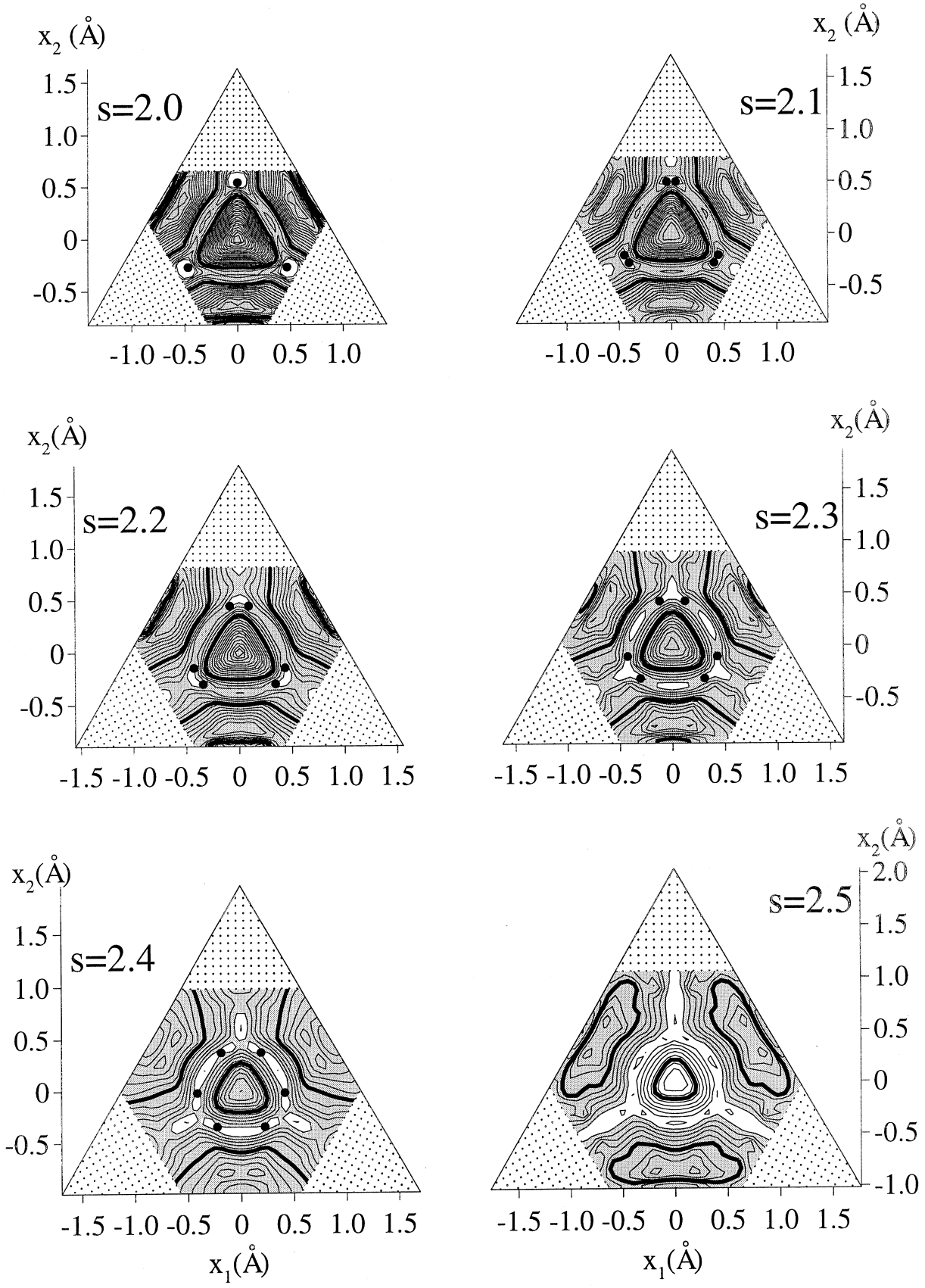

Fig. 14. a Contours of the energy difference between the $1^1A'$ PES and $2^1A'$ PES in planes normal to the x_3 axis: $s = 2.0$ Å to $s = 2.5$ Å. *Markings*: see text in Sect. 6.1.

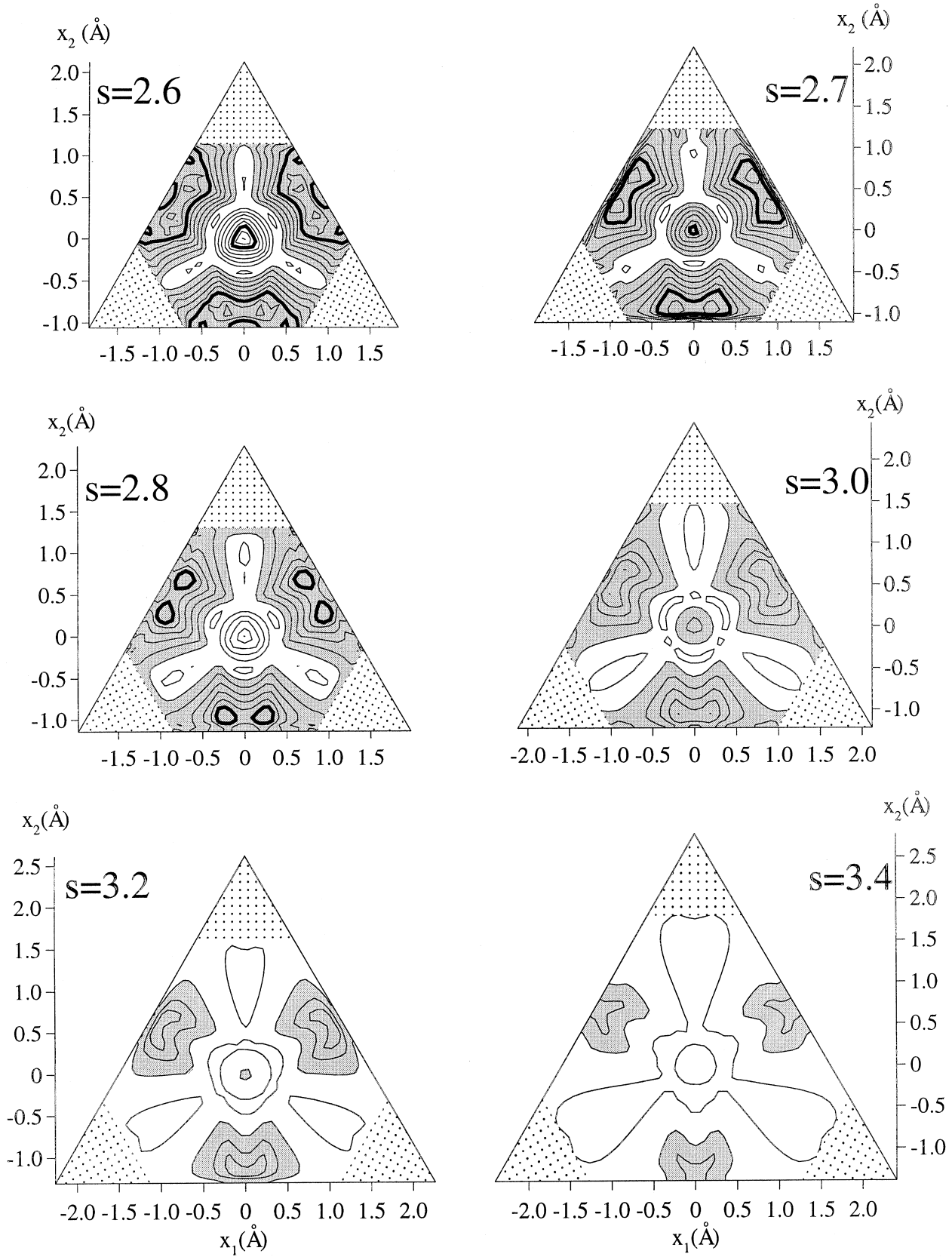

Fig. 14. b Contours of the energy difference between the $1^1A'$ PES and $2^1A'$ PES in planes normal to the x_3 axis: $s = 2.6$ Å to $s = 3.4$ Å. *Markings*: as in **a**

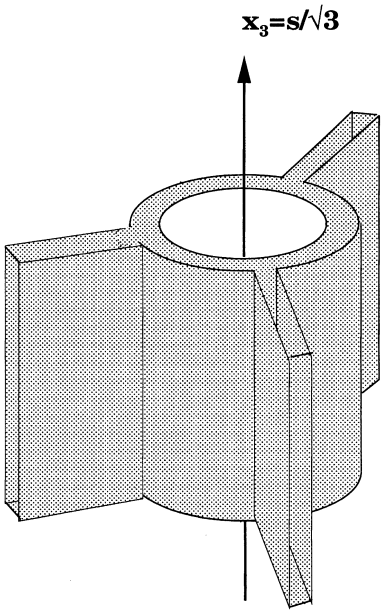

Fig. 15. Schematic diagram of the volume in the perimetric coordinate space within which the $1^1A'$ and $2^1A'$ PES are close to each other

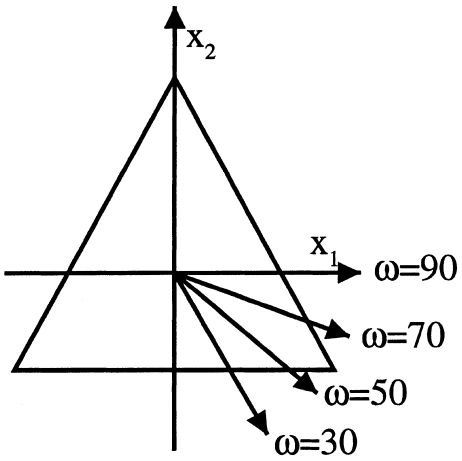

Fig. 16. Definition of angles w in x_1–x_2 space

sponding to one of the end atoms separating off. The excited state does not have a ring minimum, but it does have three open minima. Their geometries are close to those of the aforementioned transition states between the ground state minima. The six dissociation paths of the excited state are similar to those of the ground state.

Both states dissociate into the same state of $O_2 + O$, viz., the ground states of the separated system $[O(^3P + O_2(^3\Sigma_g^-)]$, whose energy lies in between the energies of the open minima of the $1^1A'$ and $2^1A'$ PES of O_3. The excited state is therefore metastable with a dissociation barrier of about 13 kcal/mol. The ground state energy rises very sharply along the dissociation reaction path, reaching the energy of $(O_2 + O)$ when one of the two O_3 bonds has stretched to only 33% beyond the equilibrium distance. It probably has a small barrier towards dissociation.

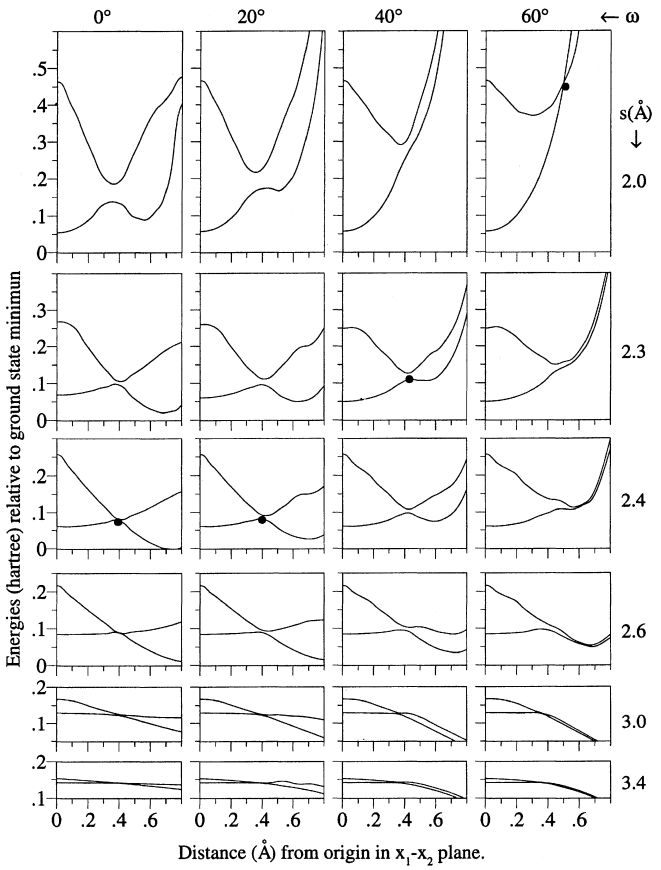

Fig. 17. Energies of the $1^1A'$ and $2^1A'$ states along lines $x_2/x_1 = \tan\omega$ for various angles ω

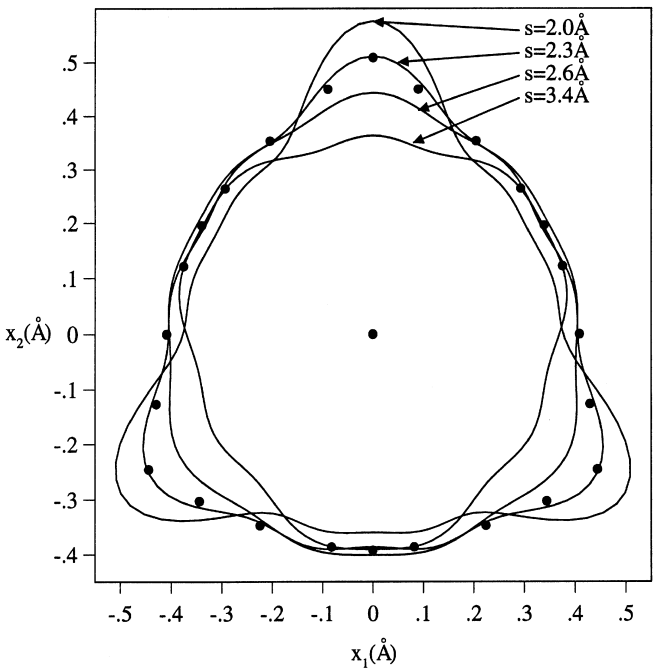

Fig. 18. Curves of closest approach between $1^1A'$ and $2^1A'$ PES in the cylinder section of Fig. 15 for four values of s. *Dots* mark the projection of the actual intersection seam

The paths towards isomerization between the open minima start out close to the dissociative paths and then split off from them. Such isomerizations are, however, highly unlikely on the ground state surface, whereas they are not improbable on the excited state surface.

There exists an extended region in coordinate space, of a distinctive shape (see Figs. 15 and 16), where the two states come very close. In fact, the two states intersect within this region along a seam which consists of four branches which are connected in three knots. This is discussed in the companion paper [9b]. Radiationless transitions can therefore be expected to occur over a wide region in coordinate space.

For isosceles confirmations with obtuse apex angles, both states belong to the same irreducible representation in C_{2v}, viz., $^1A_1$. However, for isosceles confirmations with very acute angles, the two states belong to different C_{2v} irreps, namely $^1A_1$ and $^1B_2$. Hence, a complete elucidation in C_{2v} would call for the simultaneous consideration of the three states $1^1A_1, 2^1A_1$, and 1^1B_2, all of which become $^1A'$ states when the symmetry is lowered to C_s.

Acknowledgements. This work was supported by the Division of Chemical Sciences, Office of Basic Energy Sciences, US Department of Energy (USDOE). The Ames Laboratory is operated for the USDOE by Iowa State University under Contract no. W-7405-Eng-82.

References

1. Steinfeld JI, Adler-Golden SM, Gallagher JW (1987) J Phys Chem Ref Data (Am Chem Soc and Am Inst Phys for US Natl Bur Standards) 16:911
2. Hay PJ, Dunning, Jr. TH (1977) J Chem Phys 67:2290
3. Wright JS, Shih S, Buenker RJ (1980) Chem Phys Lett 75:513
4. Wilson, Jr. CW, Hopper DG (1981) J Chem Phys 74:59
5. Hay PJ, Pack RT, Walker RB, Heller EJ (1982) J Phys Chem 86:862
6. Sheppard MG, Walker RB (1983) J Chem Phys 78:7191
7. Jones RO (1984) J Chem Phys 82:325
8. Banichevich A, Peyerimhoff SD, Grein F (1990) Chem Phys Lett 173:1

9a. Xantheas S, Atchity GJ, Elbert ST, Ruedenberg K (1991) J Chem Phys 94:8054

9b. Atchity G, Ruedenberg K (1997) Theor Chem Acc 96:195–204

10. Nordfors D, Agren H, Jorgen H, Jensen AA (1991) Int J Quant Chem XL:475
11. Braunstein M, Hay PJ, Martin RL, Pack RT (1991) J Chem Phys 95:8239
12. Banichevich A, Peyerimhoff SD, Beswick JA, Atabek O (1992) J Chem Phys 96:6580
13. Yamashita K, Morokuma K, LeQuere F, Leforestier C (1992) Chem Phys Lett 191:515
14. Banichevich A, Peyerimhoff SD (1993) Chem Phys 174:93
15. Domcke W, Woywood C (1993) Chem Phys Lett 216:362
16. Leforestier C, LeQuere F, Yamashita K, Morokuma K (1994) J Chem Phys 101:3806
17. Tsuneda T, Nakano H, Hirao K (1995) J Chem Phys 103:6520
18. Dunning TH Jr (1989) J Chem Phys 90:1007
19. A good review of MCSCF methods is by Shepard R (1978) In:Ab Initio methods in quantum chemistry II. Wiley, Chichester, p 63. See also Roos BO ibid, p 399
20. Werner HJ, Knowles PJ (1985) J Chem Phys 82:5053; Chem Phys Lett 115:259
21. Atchity G, Ruedenberg K (1997) Theor Chem Acc 96:205–211
22. Franke R, Nielson GM (1991) In:Hagen H, Roller D (eds) Geometric modeling. Springer, New York, p 131
23. de Boor C (1978) A Practical guide to splines. Springer, New York
24. Franke R (1982) Math Comp 38:181
25. Akima H (1978) Algorithm 526 in ACM TOMS 4:160
26. Renka R (1988) Algorithm 660 in ACM TOMS 14:149
27. Franke R (1982) Comp Maths Appls 8:273
28. Standard JM Poster 236, 211th American Chemical Society National Meeting and Exposition, New Orleans, 24–28 March 1996
29. Werner HJ, Reinsch EA (1982) J Chem Phys 76:3144; Werner H J (1987) Adv Chem Phys 59:1
30. Lee TJ, Scuseria GE (1993) J Chem Phys 93:489
31. Stanton JF, Bartlett RJ, Magers DH, Lipscomb WN (1989) Chem Phys Lett 163:333
32. Valtazanos P, Ruedenberg K (1986) Theor Chem Acta 69:281
33. Atchity GJ, Xantheas SS, Ruedenberg K (1991) J Chem Phys 95:1862